Chemical Engineering Journal 472 (2023) 144873

Contents lists available at ScienceDirect

Chemical Engineering Journal

journal homepage: www.elsevier.com/locate/cej

Enantioselective inorganic nanomaterials with near-infrared circular-polarized-activated photothermal response

Yarong Gu [a,b], Yuchao Du [a], Wenhe Wang [a], Xiaosheng Fang [b,c], Ziqing Li [c,*], Lijuan Zhao [a,*]

[a] Materials Genome Institute, Shanghai University, Shanghai 200444, PR China
[b] Department of Materials Science, State Key Laboratory of Molecular Engineering of Polymers, Fudan University, Shanghai 200433, PR China
[c] Shanghai Frontiers Science Research Base of Intelligent Optoelectronics and Perception, Institute of Optoelectronics, Fudan University, Shanghai 200433, PR China

ARTICLE INFO

Keywords:
Copper sulfide
Chiral inorganic nanomaterials
Enantioselectivity
Photothermal

ABSTRACT

Chiral inorganic semiconductor materials have great potential in chiral catalysis, biomedicine and chiroptical devices. However, the narrow chiroptical response and weak chiroptical intensity limit their development. Herein, chiral CuS (D-/L-CuS) were prepared by a facile ligand exchange method using alanine (Ala) and penicillamine (Pen), respectively. The properties and stereostructures of chiral ligands resulted in enantioselectivity and chiroptical activity from ultraviolet to near-infrared (NIR) of chiral CuS. And the maximum of asymmetry factor |g| was up to 1.02×10^{-2}, which is far higher than those of most chiral ligand-modified inorganic semiconductor nanomaterials. The NIR chiroptical activity facilitated photothermal performance, which could be tuned by circularly polarized light (CPL). D-CuS showed higher photothermal efficiency under right CPL radiation, while L-CuS showed higher photothermal efficiency under left CPL radiation. L-Pen-CuS exhibited the highest photothermal conversion efficiency of 22.18% under left CPL radiation. Moreover, the underlying mechanism of chirality in CuS was revealed for the first time. The coupling of amino acid ligands and CuS through Coulomb interactions allowed chiral transfer, and the orbital hybridization of chiral ligand orbitals with CuS molecular orbitals transferred chiral information. This work will further promote the understanding of induced chirality in inorganic semiconductor materials and the application of chiroptical-active inorganic semiconductor materials.

1. Introduction

Circular dichroism (CD) caused by the different absorption of left circularly polarized light (LCPL) and right circularly polarized light (RCPL) in chiral materials is one of their important properties [1,2]. The chiroptical responses of most biomolecules usually exist in the ultraviolet (UV) region, which cannot meet the needs of a wide range of CD detections and applications. Inorganic semiconductor materials have tunable optical properties and are widely used in photodetectors, biomedicine and other optoelectronic fields [3–10]. Most of the studied chiral inorganic semiconductor nanomaterials (CdSe, HgS, etc.) have strong biotoxicity, narrow chiroptical response, and weak chiroptical intensity, which limits their practical applications. Thus, it is essential to explore novel chiroptical-active and favorably biocompatible nanomaterials.

Copper sulfide (CuS) is known for having significant optical absorption from UV to near-infrared (NIR) that can be associated with electronic transitions, charge transfer, and localized surface plasmon resonance (LSPR) effects [11–14]. The NIR absorbance and low biological toxicity make it promising in the fields of cancer therapy, sensing and so on [15–17]. Therefore, CuS NPs may have great potential in the development of high-performance chiral inorganic semiconductor materials. There are few reports on the preparation and application of chiral CuS so far. In 2014, J. Govan et al. first prepared penicillamine (Pen) stabilized chiral CuS nanoparticles (NPs) which exhibited CD mirror signals at the UV–vis region of 320–600 nm [18]. Later, Kuang group reported that chiral $Cu_{2-x}S$ quantum dots can catalyze protein cleavage under circularly polarized light (CPL), and L-$Cu_{2-x}S$ showed the highest catalytic performance under LCPL irradiation [19]. Recently, they found that $Cu_{1.96}S$ NPs can site-selectively cleave capsid in tobacco mosaic virus, which can be used as effective antiviral agents [20]. However, the mechanism of induced chirality in CuS is unclear, and there is still plenty of room for investigation of chiroptical-active CuS.

The combination of chiral ligands and inorganic semiconductor

* Corresponding authors.
E-mail addresses: lzq@fudan.edu.cn (Z. Li), zhaolijuan@t.shu.edu.cn (L. Zhao).

https://doi.org/10.1016/j.cej.2023.144873
Received 11 May 2023; Received in revised form 13 July 2023; Accepted 16 July 2023
Available online 17 July 2023

materials with LSPR effect can greatly expand the response range and enhance the chiral response signal [21,22]. Here, alanine (Ala) and Pen were selected to prepare chiral CuS by ligand exchange method because they are nonpolar and polar amino acids, respectively. Meanwhile, the strong coordinative bond between Cu atoms of CuS and S atoms of the thiol in Pen may have contributed to strong CD activity. Ala modified CuS and Pen modified CuS exhibited different morphologies, optical activities, and enantioselectivities, which are related to the properties and stereostructures of chiral ligand itself. Moreover, the photothermal responses of chiral CuS in NIR region could be regulated with CPL because chiroptical-active CuS had different absorption of LCPL and RCPL. The underlying mechanism of chirality for amino acid modified CuS was described in terms of the hybrid orbital theory and the Coulomb interactions.

2. Experimental section

2.1. Chemicals

Copric chloride dihydrate ($CuCl_2{\cdot}2H_2O$), sodium sulfide nonahydrate ($Na_2S{\cdot}9H_2O$), D-Penicillamine ($C_5H_{11}NO_2S$, D-Pen) and L-Penicillamine ($C_5H_{11}NO_2S$, L-Pen) were purchased from Aladdin. D-Alanine ($C_3H_7NO_2$, D-Ala) and L-Alanine ($C_3H_7NO_2$, L-Ala) were purchased from Science Peptide Co., Ltd. (Shanghai, China). Sodium citrate ($C_6H_5Na_3O_7$, Na_3cit) and hydrogen peroxide (H_2O_2) were purchased from Sinopharm Chemical Reagent Co., Ltd. Sodium phosphate monobasic (H_2NaPO_4), D-DOPA ($C_9H_{11}NO_4$) and L-DOPA ($C_9H_{11}NO_4$) were purchased from Sigma Aldrich. All chemical were used without further purification.

2.2. Synthesis of chiral CuS

Cit-CuS NPs were first prepared as previously reported [23]. 10.77 mg of $CuCl_2{\cdot}2H_2O$ and 10 mg of Na_3cit were mixed into 50 mL ultrapure (UP) water. Then 37.196 mg of $Na_2S{\cdot}9H_2O$ was added and stirred for 5 min. The above mixed solution was transferred to an oil bath at 90 °C for 15 min to obtain an aqueous solution of cit-CuS NPs. Subsequently, chiral CuS NPs were obtained by ligand exchange using different amino acids. Different amounts of D-/L-Ala (or D-/L-Pen) were added to 12 mL cit-CuS NPs aqueous solution to obtain the amino acid concentration of 2.5 mM, 5 mM, 7.5 mM, 12.5 mM and 20 mM, respectively. The mixed solutions were sonicated for 5 min to achieve the exchange reaction between achiral citrate and chiral amino acids. Then, the solutions were aged in the dark for 24 h. To purify the products, the product will be dialyzed with 0.5–1 KD membrane in UP water for 3 days to remove excess reactants. The samples were successively named D-/L-Ala-CuS-1, D-/L-Ala-CuS-2, D-/L-Ala-CuS-3, D-/L-Ala-CuS-4 and D-/L-Ala-CuS-5 (or D-/L-Pen-CuS-1, D-/L-Pen-CuS-2, D-/L-Pen-CuS-3, D-/L-Pen-CuS-4 and D-/L-Pen-CuS-5) according to the concentration of amino acids.

2.3. Characterization

X-ray diffraction (XRD) pattern of the sample was carried out on a PANalytical Empyrean X-ray diffractometer using a Cu Kα radiation (λ = 1.54060 Å). Raman spectra was performed on a confocal Raman scattering system with a 532 nm laser. Transmission electron microscope (TEM) and high angle annular dark field-scanning transmission electron microscope (HAADF-STEM) images were recorded using a Titan ETEM transmission electron microscope equipped with an energy dispersive spectroscopy (EDS). The X-ray surface photoelectron spectra (XPS) measurements were performed on a Thermo fisher EscaLab250Xi system. Fourier Transform infrared (FT-IR) spectra were measured by a Nicolet iS50 Spectrum of Thermo Fisher with a spectral range of 500–4000 cm^{-1}. The samples were prepared by the conventional KBr pellet method. CD and absorption spectra were carried out on a JASCO J-1500 spectropolarimeter with scanning rate of 200 nm min^{-1} ranging from 200 to 800 nm. Time-dependent absorption spectra of DOPA were performed on a Lambda 750 UV–vis spectrophotometer. The pH was measured by a FiveEasy Plus FE28 pH meter of Mettler Toledo.

2.4. DOPA oxidation studies

The catalytic effect of CuS NPs sample on DOPA oxidation were carried out by using the time process mode to monitor the absorbance change at 475 nm. Experiments were conducted using 1600 μL chiral CuS NPs solutions with 100 μL L-DOPA (or D-DOPA, 200 mM) as substrate in 200 μL buffer solutions (NaH_2PO_4, 200 mM, pH 4.22, room temperature) with 100 μL H_2O_2 (1 M). As a control, 1600 μL UP water was used to replace chiral CuS NPs solutions for testing under the same conditions.

2.5. Photothermal characterization

The photothermal performance of chiral CuS was characterized under linearly polarized lights (LPL), LCPL and RCPL by an 808 nm NIR laser (LSR808H, Q-BAIHE, Wuhan, China). The solution was irradiated for 600 s with a power density of 1.5 W cm^{-2} and then cooled down to room temperature naturally. The same volume UP water was used in the control group. The temperature was measured every 20 s by an infrared imaging device.

3. Results and discussion

3.1. Materials characterization

Before ligand exchange using amino acids, homochiral cit-CuS NPs with negative CD signals (Fig. S1) were prepared by the same method in our previous report [24]. XRD pattern demonstrated that cit-CuS NPs were hexagonal CuS with a space group of P63/mmc (JCPDS #06-0464). The TEM image showed that the cit-CuS NPs were nanoparticles with an average size of about 20 nm. When chiral Ala and Pen were used as chiral ligands, respectively, the obtained chiral CuS exhibited different morphologies and sizes. The samples carrying D-/L-Ala had a larger average size (ca. 40 nm), and the nanoflower (NF) structure composed of many nanoflakes can be clearly observed from HAADF-STEM (Fig. 1a,b and Fig. S2a, b). EDS elemental mapping and XPS results demonstrated that Ala was successfully modified on the surface of CuS NFs. It can be observed from the EDS mapping (Fig. 1c and Fig. S2c) that Cu, S, and C elements were uniformly distributed on the surface of the sample, and the C elements were derived from the chiral Ala molecules modified on the sample surface. The XPS measured spectra and curve fitting of Cu 2p, S 2p, and N 1s were shown in Fig. 1g–i and Figure S3a, where the XPS spectra were calibrated to the standard C 1s at a binding energy of 284.8 eV. Two strong peaks at 932.0 eV and 951.9 eV were observed in the Cu 2p spectra of D-/L-Ala-modified CuS, attributed to Cu^+ $2p_{3/2}$ and Cu^+ $2p_{1/2}$, respectively, which correspond to the Cu oxidation state in covellite CuS [25,26]. At the same time, two weak peaks at 933.6 eV and 953.5 eV observed in D-Ala modified CuS were assigned to Cu^{2+} $2p_{3/2}$ and Cu^{2+} $2p_{1/2}$, respectively, with a splitting energy separation equal to 19.9 eV, indicating the existence of Cu^{2+} in hexagonal CuS [27]. The S 2p results showed the typically mixed valence states of S in covellite CuS, in which the peaks at 161.8 eV and 162.9 eV were assigned to S^{2-} $2p_{3/2}$ and S^{2-} $2p_{1/2}$, while the peaks at 163.6 eV and 164.5 eV were assigned to $(S_2)^{2-}$ $2p_{3/2}$ and $(S_2)^{2-}$ $2p_{1/2}$ [28–30]. The results of Cu 2p and S 2p spectra manifested the successful formation of CuS. It is worth noting that the peak at 168.0 eV originated from SO_4^{2-}, indicating that a small amount of S^{2-} on the sample surface was oxidized. This was due to the common fact that water adsorbed on the nanoparticle surface facilitated the conversion of sulfide ions to sulfate ions in the presence of oxygen molecules [25]. Furthermore, the peak at 399.5 eV in the N 1s spectra can be attributed to N-H and C-N, while the peak at 400.7 eV was attributed to C-N [31]. Neither sodium

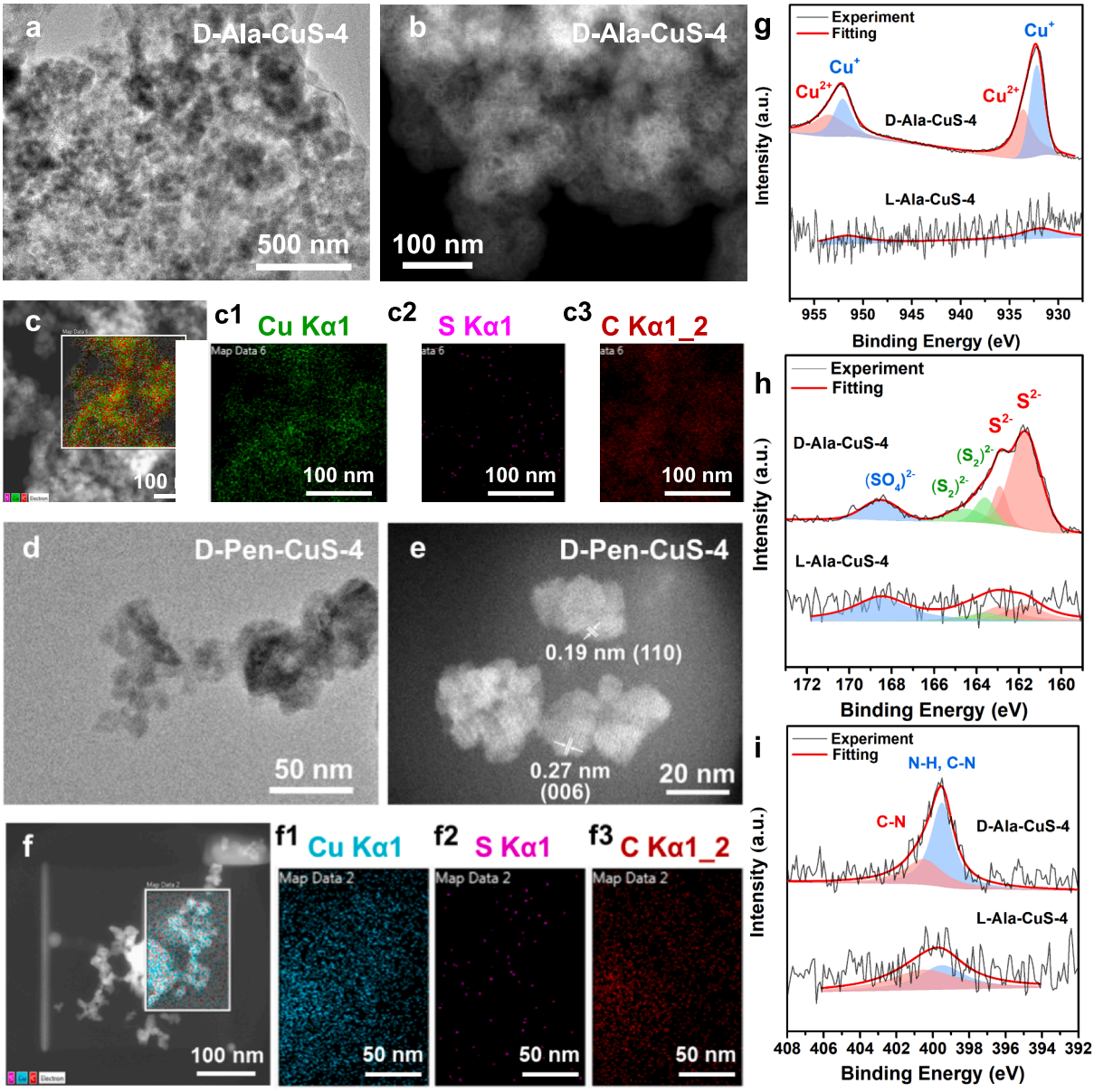

Fig. 1. Characterization of D-Ala-CuS-4 and D-Pen-CuS-4: (a) TEM image, (b) HAADF-STEM image, and (c) EDS mapping of D-Ala-CuS-4, (c1), (c2) and (c3) are for Cu, S and C elements, respectively. (d) TEM image, (e) HAADF-STEM image, and (f) EDS mapping of D-Pen-CuS-4, (f1), (f2) and (f3) are for Cu, S and C elements, respectively. (g-i) XPS spectra of D-/L-Ala-CuS-4 of Cu 2p, S 2p and N 1s.

citrate nor CuS had N—H and C—N bonds, so these two peaks could be derived from Ala, which confirmed Ala was successfully modified on the surface of CuS. Since the XPS signal was concentration dependent, dialysis purification not only removed free chiral molecules from the original sample but also sacrificed sample concentration, resulting in small XPS peaks. To further prove the composition of D-/L-Ala-CuS-4, the XPS spectra of pristine Ala-CuS-4 were provided (Fig. S3), and stronger signals consistent with Ala-CuS-4 can be observed. Unlike the nanoflowers of Ala modified CuS, Pen modified samples maintained the nanoparticles morphology of pristine cit-CuS, with an average diameter of about 10 nm. The effect of amino acids on the morphology of CuS NPs during ligand exchange may be related to the interaction of metal–ligand complex or the difference in formation reaction kinetics [32]. According to the HAADF-STEM images (Fig. 1d, e and Fig. S2d, e), the lattice spacings of Pen modified CuS were 0.19 nm and 0.27 nm, corresponding to the (1 1 0) and (0 0 6) lattice planes of hexagonal CuS (JCPDS #06-0464), respectively. In addition, the uniform distribution of Cu, S, and C elements throughout the measured area in the EDS mapping (Fig. 1f and Fig. S2f) confirmed the formation of Pen-modified CuS NPs, in which the C element comes from Pen molecules on the sample surface. The combination forms of Ala and Pen with CuS will be studied by FT-IR in subsequent mechanism analysis.

3.2. Chiroptical properties

CD measurements were then performed to study the chiroptical activity of Ala-CuS NFs and Pen-CuS NPs. Absorption and corresponding CD signals of free Ala and Pen were located around 203 and 225 nm in the UV region, respectively (Fig. S4). The CD spectra of Ala-CuS NFs had a strong signal in the 236 nm and a weak signal in 700–800 nm region where they exhibited absorption (Fig. 2a, b and Fig. S5a, b). The negative CD peak in the UV region was consistent with that of CuS itself (Fig. S1c), and the weak signal in the NIR region could be attributed to the LSPR effect of CuS [33]. Notably, Ala-CuS before purification exhibited a mirror CD signal around 600 nm (Fig. S6). The “disappearance” of the mirror signal in Ala-CuS was due to the dialysis process

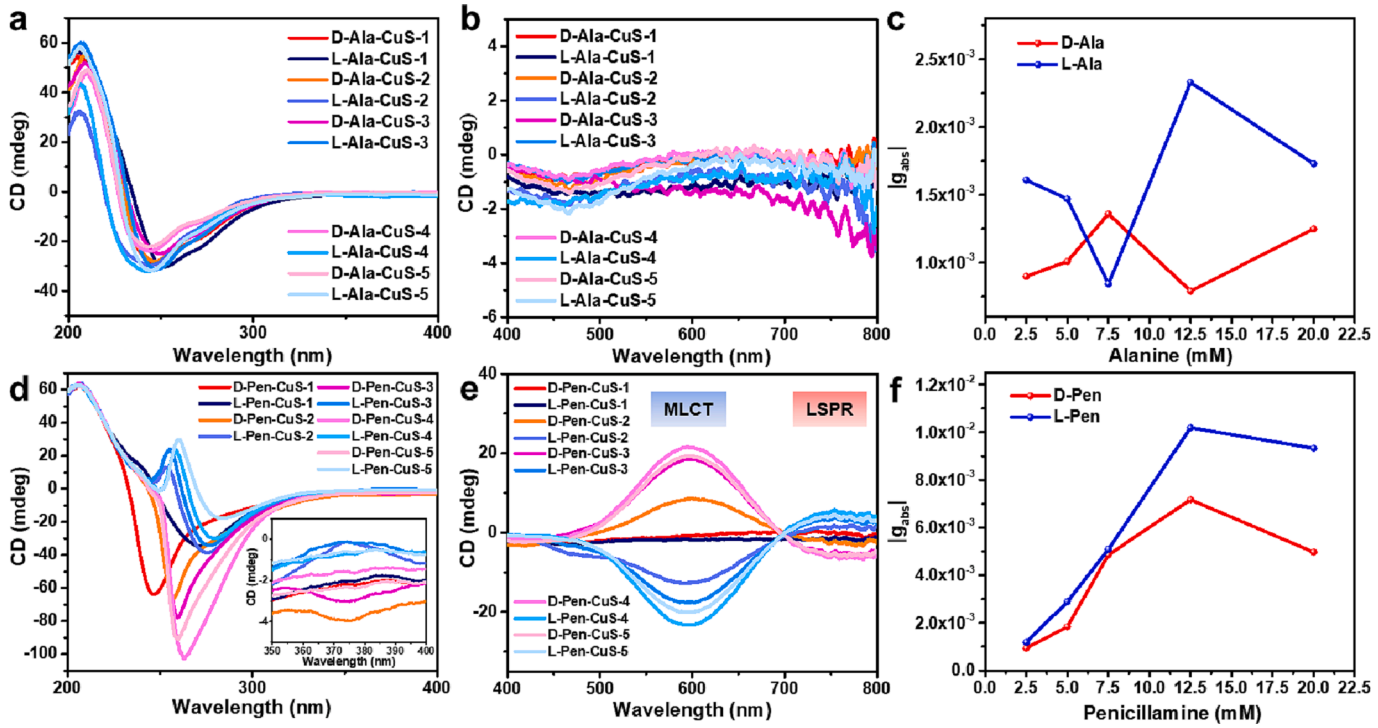

Fig. 2. Optical characterizations of chiral Ala-CuS and Pen-CuS: CD spectra of Ala-CuS in the range of (a) 200–400 nm and (b) 400–800 nm. (c) The maxima of |g| for different concentration of Ala capped CuS. CD spectra of Pen-CuS in the range of (d) 200–400 nm and (e) 400–800 nm, the inset is the magnified CD spectra in the range of 350–400 nm. (f) The maxima of |g| for different concentration of Pen capped CuS.

improved the sample purity at the expense of solution concentration, whereas the intensity of CD signals was concentration dependent [34]. To quantitatively evaluate the chiroptical activity of Ala-CuS NFs, their CD anisotropic factors (g factors) were calculated as g = ΔA/A≈CD [mdeg]/(32980·A), where ΔA is the absorbance difference of LCPL and RCPL, and A is the absorbance of the unpolarized light [35]. The g-factor spectra were plotted in Fig. S7. Among all samples (Fig. 2c), L-Ala-CuS-4 had a largest |g| value of 2.33×10^{-3}, which is higher than that of the homochiral cit-CuS NPs (1.24×10^{-3}) before ligand exchange with Ala [24]. Additionally, Ala-CuS NFs with varying concentrations of Ala had different and no-trend g-factor. This is because of the geometry-dependent nature of the chiral properties [36], since the morphology of Ala-CuS NFs was highly random (Fig. 1a–c and Fig. S2a–c). Different from the CD of Ala-CuS NFs, Pen modified CuS NPs showed strong CD mirror signals not only in the UV range, but also in the visible and NIR range corresponding to their absorbance (Fig. 2d, e and Fig. S5c, d). The mirror signals near 260 nm were attributed to the Pen on the surface of CuS, while the bisignate signals with two peaks at 595 and 750 nm resulted from the metal-to-ligand charge transfer (MLCT) effect and LSPR effect, respectively. All D-/L-Pen-CuS samples exhibited negative CD signals near 280 nm, which was considered to be derived from CuS. Due to the interaction between Pen molecules and CuS, the negative CD signal of CuS was blue-shifted, and overlapped with the CD signal induced by D-Pen, resulting in the stronger negative CD signal of the D-Pen-CuS sample near 280 nm than that of the L-Pen-CuS sample. According to the g-factor spectra (Fig. 2f and Fig. S8), the g factor increased with the concentration of Pen within a certain range and decreased when Pen concentration increased further in Fig. 2f. It can be attributed to the fact that instead of increasing the possibility for combining with CuS, an excess of chiral molecules in the solution will inhibit the combination and CD in chiral CuS [36]. Hence, regulating the concentration of chiral amino acids provides an effective way to adjust the induced chirality for potential applications. Moreover, the maximum of |g| value of L-Pen-CuS-4 is up to 1.02×10^{-2}, which is comparable to that of Pen modified $Cu_{2-x}S$ quantum dots (1.0×10^{-2}) [19]. It is an order of magnitude higher than that of Ala-CuS, and also higher than that of most chiral ligand-modified inorganic semiconductor nanomaterials, such as N-acetylcysteine modified α-HgS (1.7×10^{-3}) [37] and cysteine modified CdSe@CdS nanorods (5.2×10^{-4}) [38]. Therefore, D-/L-Ala-CuS-4 and D-/L-Pen-CuS-4 were selected for the subsequent studies.

3.3. Enantioselective reactions with DOPA enantiomers

The peroxidase-like activity of chiroptical-active CuS was evaluated by the H_2O_2-mediated oxidation of DOPA enantiomers because Cu^{2+} could catalyze a Fenton-like reaction [12]. As shown in Fig. 3a, the oxidation rates of D-DOPA and L-DOPA without Ala-CuS-4 were very slow, and their oxidation curves were almost horizontal lines close to zero. In the presence of Ala-CuS-4, it is apparent that both D-DOPA and L-DOPA were oxidized rapidly. More importantly, D-Ala-CuS-4 and L-Ala-CuS-4 showed a preference for catalytic DOPA enantiomers. D-Ala-CuS-4 had a better catalytic activity for L-DOPA than D-DOPA (blue dot and blue line in Fig. 3a), while L-Ala-CuS-4 had a better catalytic activity for D-DOPA than L-DOPA (red line and red dot in Fig. 3a). However, the same optically active Ala and Pen modified CuS exhibited opposite selectivity for DOPA enantiomers. For example, D-Pen-CuS-4 preferentially catalyzed D-DOPA but D-Ala-CuS-4 preferentially catalyzed L-DOPA (Fig. 3b). It was mainly caused by the opposite chiral stereostructures of the homo-chiroptical-active Ala and Pen. The structural formulas of Ala and Pen were shown at the top of Fig. 3a, b. Both D-Ala and D-Pen exhibited negative CD signals (Fig. S4a, b), but their chiral stereostructures were opposite, as well as L-Ala and L-Pen. The result suggested that substrate recognition came from chiral ligands on the surface of chiral CuS. A schematic of the enantioselective oxidation of chiral DOPA by chiral CuS was shown in Fig. 3c. The catalytic activity of chiral CuS was derived from CuS, which will catalyze the decomposition of H_2O_2 to generate hydroxyl radicals (•OH) [39], thus accelerating the oxidation of DOPA to produce dopachrome. Due to the different affinity between chiral ligands and DOPA enantiomers [40], chiral CuS exhibited enantioselectivity for DOPA enantiomers. Since the focus of our

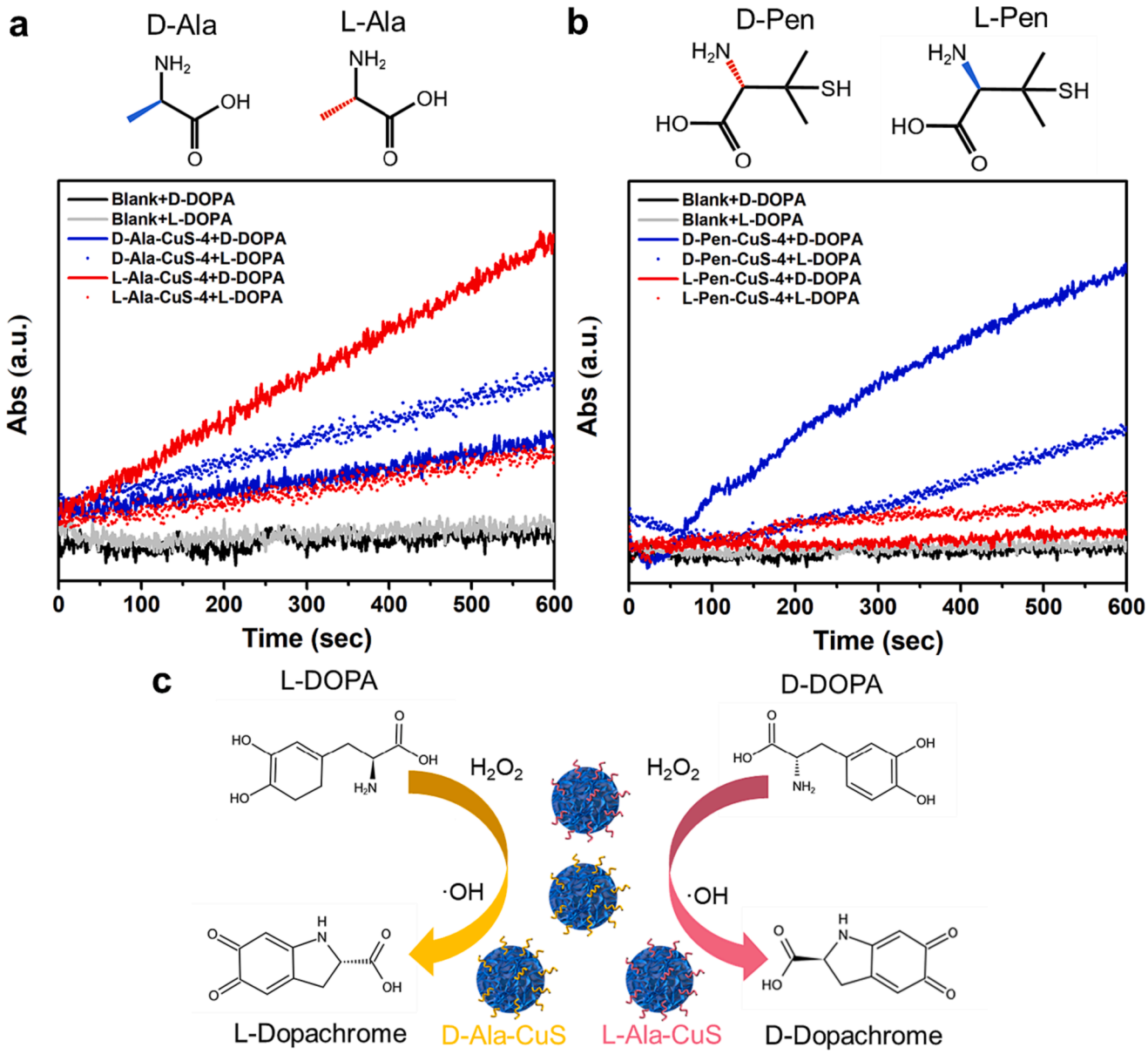

Fig. 3. The time-dependent absorbance changes of chiral DOPA at 475 nm in the absence or presence of (a) Ala-CuS-4 and (b) Pen-CuS-4 at 600 s intervals, the top are structures of Ala and Pen, respectively. (c) Enantioselective oxidation of DOPA enantiomers by Ala-CuS.

work is the enantioselectivity based on the chirality of samples, the evaluation of the catalytic activity for chiral CuS is worthy of a separate study in the future.

3.4. Photothermal performance under LPL and CPL radiation

Apart from enantioselective catalysis, the emerging CD signals in the NIR region of chiral CuS inspired us to explore their photothermal performances under CPL, which may provide a promising platform for tumor therapy with synergistic chemodynamic therapy and photothermal therapy. Compared to other wavelength ranges where light is difficult to penetrate biological tissues due to scattering and absorption, NIR radiation can penetrate deeper biological tissue, allowing subcutaneous tumor treatment [41]. Therefore, we chose 808 nm laser, one of the most commonly used light sources in photothermal therapy, for photothermal experiments. All the measurements were performed under constant stirring to achieve uniform temperature distribution upon laser irradiation, and a CPL generator was constructed to verify the CPL-responsive photothermal behaviors (Fig. 4a, b). The 808 nm laser beam passed through a polarizer to generate LPL, which transformed into LCPL or RCPL through a quarter-wave plate (QWP) with a rotation angle of −45° or 45°. And an infrared thermal imager was used to record the immediate temperature of solution samples. The photothermal performance of chiral CuS was characterized under 808 nm of LPL, LCPL or RCPL radiations for 600 s, respectively. And the solution samples were allowed to be cooled down to room temperature naturally (Fig. 4c, d and Fig. S9a, b). To evaluate their photothermal performance quantitatively, the photothermal conversion efficiency (η) of samples was calculated by the time constants (τ) according to the cooling curve (Fig. 4e, f and Fig. S9c, d). As summarized in Table 1, D-/L-Ala-CuS-4 exhibited lower η compared to D-/L-Pen-CuS-4, which may be related to the morphology change of Ala-CuS [42]. Compared with spherical cit-CuS and D-/L-Pen-CuS, the nanoflower-like Ala-CuS had weaker absorption in the NIR as demonstrated by the absorption spectra in Fig. S1d and Fig. S5, which was not conducive to photothermal conversion, since the photothermal effect of CuS was attributed to LSPR-induced light absorption in the NIR [14]. Among all the samples, L-Pen-CuS-4 exhibited the highest η of 22.18% under LCPL, which is higher than

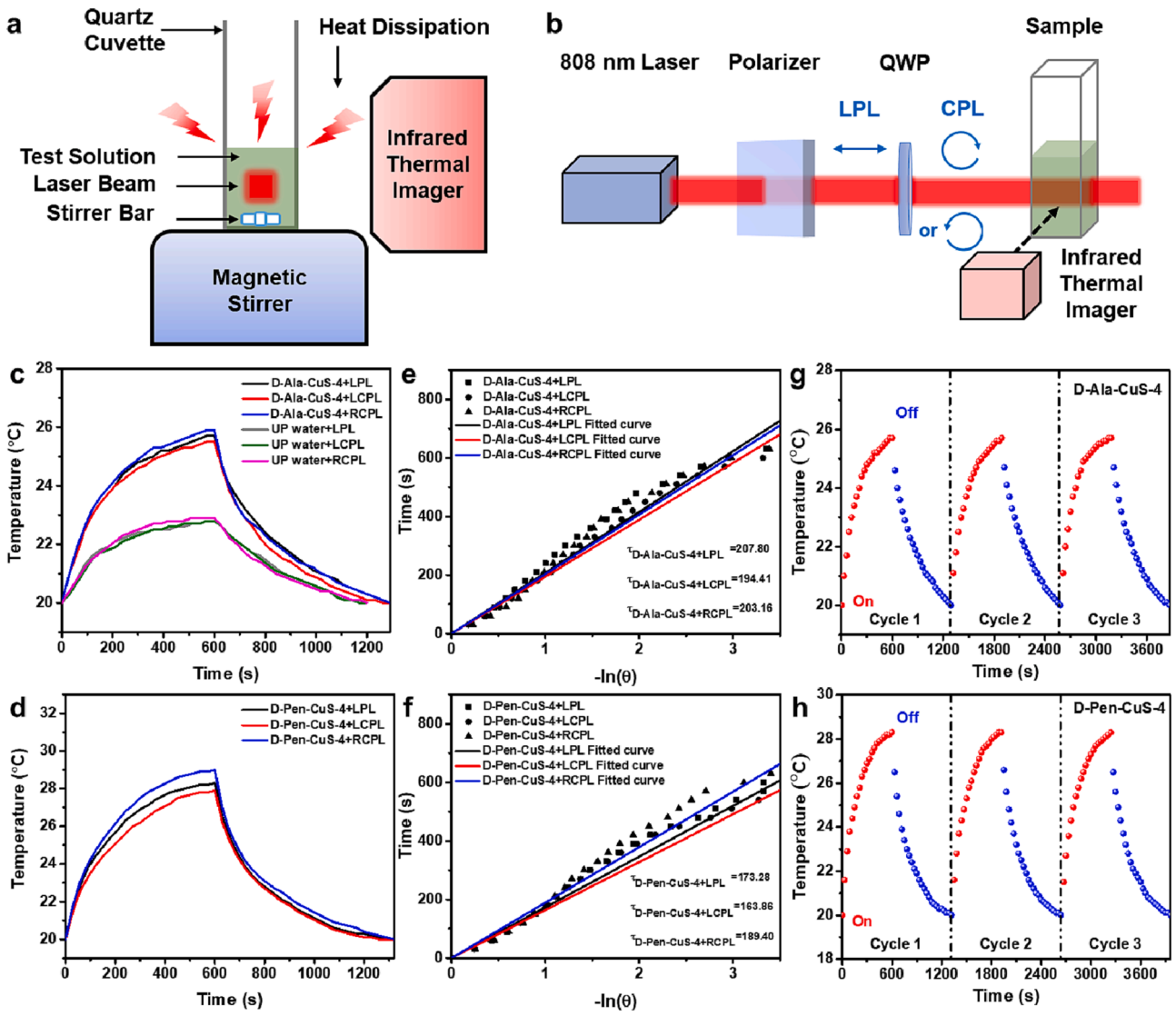

Fig. 4. Schematic illustration of (a) experimental setup for photothermal characterization and (b) the optical setup to generate CPL. All materials are not in real scale/ratio. Temperature versus time curves of (c) D-Ala-CuS-4 and (d) D-Pen-CuS-4 under 808 nm LPL/LCPL/RCPL radiation and their relaxation behaviors after turning off the laser. Linear fitting curves of (e) D-Ala-CuS-4 and (f) D-Pen-CuS-4. Thermal cycle performance curves of (g) D-Ala-CuS-4 and (h) D-Pen-CuS-4 under LPL radiation. All the lasers are measured to have the same power as 1.5 W cm^{-2} to the samples.

Table 1
Photothermal performance of Ala-CuS NFs and Pen-CuS NPs under LPL, LCPL and RCPL radiation.

Sample	τ [s]			η [%]		
	LPL	LCPL	RCPL	LPL	LCPL	RCPL
D-Ala-CuS-4 NFs	207.80	194.41	203.16	12.25	12.19	**12.96**
L-Ala-CuS-4 NFs	183.44	177.50	177.66	11.91	**12.31**	11.68
D-Pen-CuS-4 NPs	173.28	163.86	189.40	19.34	18.97	**19.63**
L-Pen-CuS-4 NPs	161.51	168.90	155.31	19.39	**22.18**	18.19

20.3% reported by Chen et al. [43], and 21.5% reported by Wang et al. [17] Moreover, D-Ala/Pen-CuS-4 obtained higher η under RCPL while L-Ala/Pen-CuS-4 obtained higher η under LCPL than under other light sources. It was consistent with chiroptical activity of D-/L-CuS in Fig. 2, implying that the D- and L-CuS adsorb more LCPL and RCPL, respectively. In addition, no apparent degradation was found during three consecutive heating/cooling processes of chiral CuS indicating that chiral CuS had good photostability (Fig. 4g, h and Fig. S9e, f). The results showed that chiral CuS achieved circular-polarized-activated photothermal activities in NIR region and were probably competent for the corresponding biomedical applications.

3.5. Mechanism analysis

As shown in Fig. 5a, the as-prepared chiral CuS has a wide chiroptical response range and a high |g| value compared with other amino acid-modified chiral inorganic semiconductor nanomaterials [37,38,44–48]. The underlying mechanism of optical chirality is described based on the hybrid orbital theory [49] and the Coulomb interactions between chiral molecules and CuS [36,50]. On the one hand, amino acid ligands and CuS were coupled through the Coulomb interactions, allowing for chirality transfer. In the previous section of materials characterization, EDS mapping and XPS spectra proved that Ala and Pen were successfully modified on the surface of CuS. Then, FT-IR spectra were used to investigate the binding form of Ala or Pen modified CuS. The vibrations near 1612 cm^{-1} and 1410 cm^{-1} in Ala were assigned to the asymmetric and symmetric vibration modes of COO–, respectively (Fig. S10). In Ala-CuS-4 samples, the asymmetric vibration band ν_{as}(C = O) and symmetric vibration band ν_{s}(C = O)

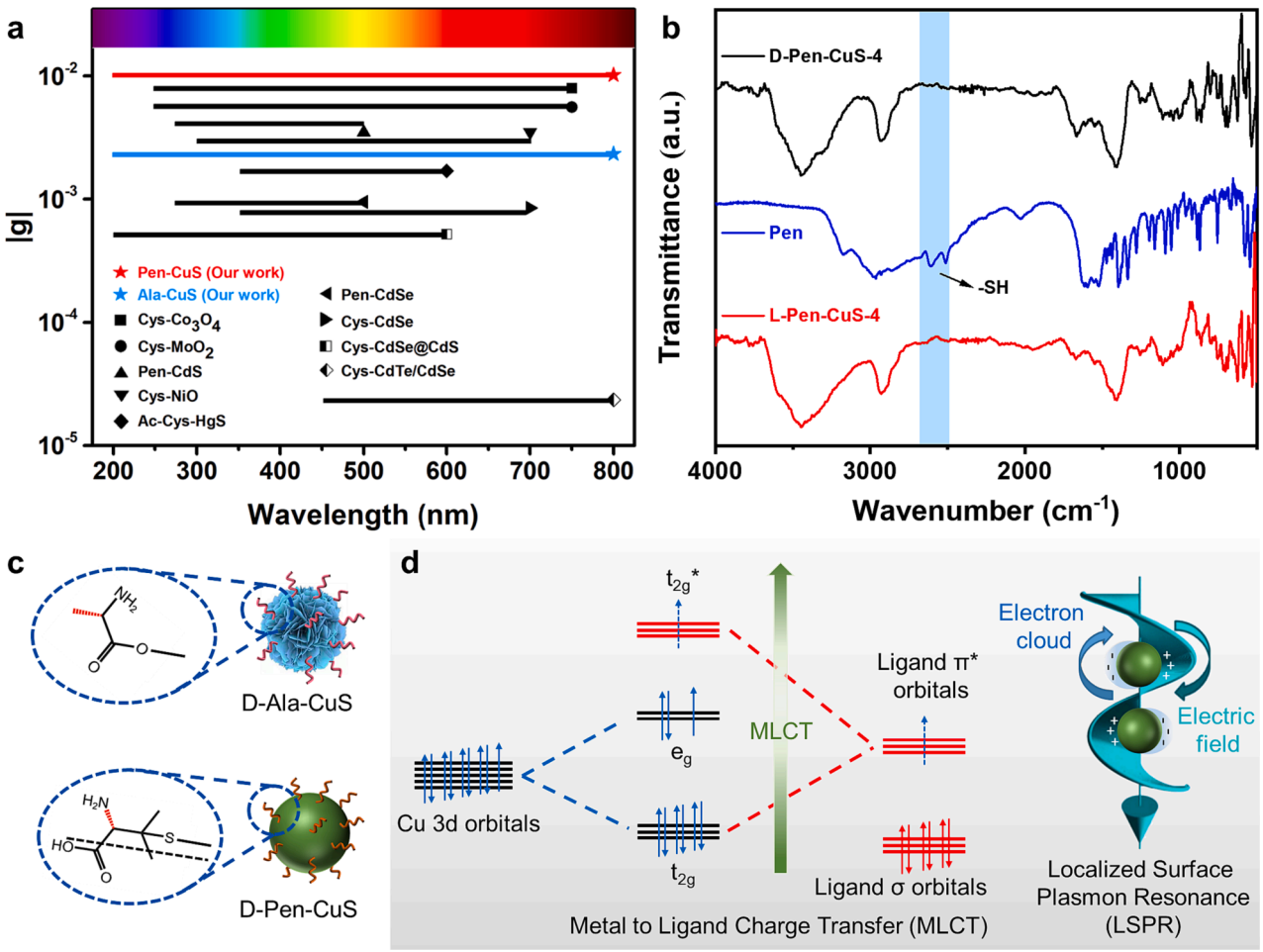

Fig. 5. (a) CD response range (lines) and maximum of the |g| factor (symboles) spectra reported for various chiral inorganic semiconductor nanomaterials modified with amino acids. The data are from Ref. 37, 38, 44, 45, 46, 47 and 48. (b) FT-IR spectra of Pen-CuS and Pen. Schematic illustration of (c) chiral D-Ala-CuS NFs and D-Pen-CuS NPs, and (d) electron transition band resulted from MLCT and LSPR.

moved to 1637 cm^{-1} and 1389 cm^{-1}, which suggested that Ala is coordinated with Cu by the COO– group [51]. For Pen-CuS-4 samples, the intensity of the peak corresponding to the -S-H groups (ca. 2612 cm^{-1}) was obviously reduced, and the peak representing hydrogen bonds (3000–4000 cm^{-1}) increased compared with Pen (Fig. 5b). This indicated that the ligands were bound to CuS surface through strong S—Cu covalent bonds and weak S—H—O hydrogen bonds [20]. Overall, the binding modes of Ala and Pen with CuS were shown in Fig. 5c. Variations in the position of ligands as well as the chemical identity of ligands impacted both the shape and anisotropy of the induced CD spectra [52]. The multidentate binding between Pen and CuS (strong S—Cu covalent bonds and weak S—H—O hydrogen bonds) could be responsible for the higher CD anisotropy than that of Ala-CuS. On the other hand, the hybridization of CuS molecular orbitals with chiral ligand orbitals transferred chiral information. Chiral CuS exhibited MLCT absorption bands in the visible region corresponding to d-d electronic transitions of Cu ions. In the octahedral field, the d orbitals of Cu ions were split into e_g orbitals with energy pushed up and t_{2g} orbitals with energy pushed down [34]. The remaining d-electrons of the Cu ions in the chiral complex t_{2g} orbital can more easily transition to the low-lying and empty π* orbital in the chiral ligand, resulting the absorption band, as illustrated in Fig. 5d. Meanwhile, the absorption of CuS in the NIR region originated from the LSPR effect, in which the conductive free electrons collectively resonate in response to the incoming electromagnetic radiation, resulting in amplified light absorption as well as scattering [14]. In the antenna effect, nanoparticles act as nanoantennas that amplify the chiral signals of weak molecules. However, the chiroptical response in the NIR region here does not originate from the antenna effect. When a nanomaterial with plasmonic effect is combined with chiral ligands, the CD signal will be generated in the plasmonic resonance frequency region of the nanomaterials due to the LSPR effect [21,33,53]. When CPL interacts with the nanoparticles, it spirally drives the electron cloud that oscillates at the frequency of the light and generates an electric current on the surface of the nanostructure [54]. It contributed to the extended CD response of chiral CuS in the NIR region and its potential applications.

4. Conclusion

In summary, chiral CuS with different chiroptical activity from UV to NIR were obtained using Ala and Pen as ligands, respectively. D-/L-Ala-CuS and D-/L-Pen-CuS showed different enantioselectivities in catalytic oxidation of DOPA, which is related to the stereostructures of Ala and Pen on the surface of CuS. In the photothermal measurements, NIR chiroptical-active CuS showed different photothermal responses under the irradiation of 808 nm LCPL and RCPL. And L-Pen-CuS-4 exhibited the highest η of 22.18% under LCPL. The origin of induced chirality was elucidated to mainly involve the Coulomb interaction and the orbital hybridization between chiral ligands and CuS. This work not only explores the potential applications of chiroptical-active CuS in chiral catalysis and cancer therapy, but also reveals the relationship between CuS and induced chiroptical activity, providing strategies for the better

understanding, rational design and application of inorganic semiconductor materials with chiroptical properties.

Declaration of Competing Interest

The authors declare the following financial interests/personal relationships which may be considered as potential competing interests: [I solemnly declare that the manuscript submitted by me is the result of my independent research work under the guidance of my supervisor. Individuals and groups that have made important contributions to the study of this paper have been clearly identified in the text. In addition to the references cited in this article, this paper does not contain any works or achievements that have been published or authored by other individuals or groups.].

Data availability

Data will be made available on request.

Acknowledgements

The work was supported by National Key Research and Development Program of China (No. 2021YFB3200804), National Key R&D Program of China (No. 2022YFA1402900), National Natural Science Foundation of China (No. 62204047 and 12061131009), Science and Technology Commission of Shanghai Municipality (No. 21520712600 and 19520744300).

Appendix A. Supplementary data

Supplementary data to this article can be found online at https://doi.org/10.1016/j.cej.2023.144873.

References

[1] L. Xiao, T. An, L. Wang, X. Xu, H. Sun, Novel properties and applications of chiral inorganic nanostructures, Nano Today 30 (2020), 100824.
[2] Y. Duan, S. Che, Chiral mesostructured inorganic materials with optical chiral response, Adv. Mater. 2205088 (2023).
[3] M. Deng, Z.Q. Li, X. Deng, Y. Hu, X.S. Fang, Wafer-scale heterogeneous integration of self-powered lead-free metal halide UV photodetectors with ultrahigh stability and homogeneity, J. Mater. Sci. Technol. 164 (2023) 150–159.
[4] X. Deng, Z. Li, F.a. Cao, E. Hong, X. Fang, Woven Fibrous photodetectors for scalable UV optical communication device, Adv. Funct. Mater. 33 (23) (2023).
[5] S. Song, D. Wang, K. Zhao, Y. Wu, P. Zhang, J. Liu, G. Yang, P. Gong, Z. Liu, Donor-acceptor structured photothermal COFs for enhanced starvation therapy, Chem. Eng. J. 442 (2022), 135963.
[6] Z.Q. Li, X. Liu, C. Zuo, W. Yang, X.S. Fang, Supersaturation-controlled growth of monolithically integrated lead-free halide perovskite single-crystalline thin film for high-sensitivity photodetectors, Adv. Mater. 33 (2021) 2103010.
[7] E. Hong, Z. Li, T. Yan, X. Fang, Surface-tension-dominant crystallization of 2D perovskite single crystals for vertically oriented hetero-/homo-structure photodetectors, Nano Lett. 22 (21) (2022) 8662–8669.
[8] Z. Li, E. Hong, X. Zhang, M. Deng, X. Fang, Perovskite-type 2D materials for high-performance photodetectors, J. Phys. Chem. Lett. 13 (5) (2022) 1215–1225.
[9] X. Zhang, Z. Li, T. Yan, L.i. Su, X. Fang, Phase-modulated multidimensional perovskites for high-sensitivity self-powered UV photodetectors, Small 19 (9) (2023) 2206310.
[10] P. Gong, J. Li, J. Wang, W. Wu, C. Li, D. Wang, J. Shi, J. Liu, F. Zhou, W. Liu, Controlled growing of graphdiyne film for friction reduction and antiwear, ACS Nano 17 (9) (2023) 8252–8261.
[11] X. Fang, T. Zhai, U.K. Gautam, L. Li, L. Wu, Y. Bando, D. Golberg, ZnS nanostructures: from synthesis to applications, Prog. Mater. Sci. 56 (2) (2011) 175–287.
[12] Y. Wang, Y. Xia, Near-infrared optically active $Cu_{2-x}S$ nanocrystals: sacrificial template-ligand exchange integration fabrication and chirality dependent autophagy effects, J. Mater. Chem. B 8 (2020) 7921–7930.
[13] K.H. Park, J. Kwon, U. Jeong, J.-Y. Kim, N.A. Kotov, J. Yeom, Broad chiroptical activity from ultraviolet to short-wave infrared by chirality transfer from molecular to micrometer scale, ACS Nano 15 (9) (2021) 15229–15237.
[14] J.M. Luther, P.K. Jain, T. Ewers, A.P. Alivisatos, Localized surface plasmon resonances arising from free carriers in doped quantum dots, Nat. Mater. 10 (5) (2011) 361–366.
[15] S. Goel, F. Chen, W. Cai, Synthesis and biomedical applications of copper sulfide nanoparticles: from sensors to theranostics, Small 10 (2014) 631–645.
[16] M. Liu, Y. Liu, B. Gu, X. Wei, G. Xu, X. Wang, M.T. Swihart, K.-T. Yong, Recent advances in copper sulphide-based nanoheterostructures, Chem. Soc. Rev. 48 (19) (2019) 4950–4965.
[17] S. Wang, Y. Pang, S. Hu, J. Lv, Y. Lin, M. Li, Copper sulfide engineered covalent organic frameworks for pH-responsive chemo/photothermal/chemodynamic synergistic therapy against cancer, Chem. Eng. J. 451 (2023), 138864.
[18] J. Govan, A. Loudon, A.V. Baranov, A.V. Fedorov, Y.K. Gun'ko, Chiral quantum dot based materials, Nanophotonics V. SPIE 9126 (2014) 183–195.
[19] C. Hao, R. Gao, Y. Li, L. Xu, M. Sun, C. Xu, H. Kuang, Chiral semiconductor nanoparticles for protein catalysis and profiling, Angew. Chem. Int. Ed. Engl. 131 (22) (2019) 7449–7452.
[20] R. Gao, L. Xu, M. Sun, M. Xu, C. Hao, X. Guo, F.M. Colombari, X. Zheng, P. Král, A. F. de Moura, C. Xu, J. Yang, N.A. Kotov, H. Kuang, Site-selective proteolytic cleavage of plant viruses by photoactive chiral nanoparticles, Nat. Catal. 5 (2022) 694–707.
[21] Y. Wen, M.Q. He, Y.L. Yu, J.H. Wang, Biomolecule-mediated chiral nanostructures: a review of chiral mechanism and application, Adv. Colloid Interface Sci. 289 (2021), 102376.
[22] Y. Zhu, M. Guan, J. Wang, H. Sheng, Y. Chen, Y. Liang, Q. Peng, G. Lu, Plasmon-mediated photochemical transformation of inorganic nanocrystals, Appl. Mater. Today 24 (2021), 101125.
[23] W. Gao, Y. Sun, M. Cai, Y. Zhao, W. Cao, Z. Liu, G. Cui, B. Tang, Copper sulfide nanoparticles as a photothermal switch for TRPV1 signaling to attenuate atherosclerosis, Nat. Commun. 9 (2018) 231.
[24] Y. Gu, Y. Jiang, J. Chen, C. Gao, L. Feng, J. Wu, L. Zhao, Circular dichroism and enantio-selective catalytic effect of copper sulfide, Opt. Mater. 132 (2022), 112787.
[25] H. Wu, V.W. Or, S. Gonzalez-Calzada, V.H. Grassian, CuS nanoparticles in humid environments: adsorbed water enhances the transformation of CuS to $CuSO_4$, Nanoscale 12 (2020) 19350–19358.
[26] M. Baláž, E. Dutková, Z. Bujňáková, E. Tóthová, N.G. Kostova, Y. Karakirova, J. Briančin, M. Kaňuchová, Mechanochemistry of copper sulfides: characterization, surface oxidation and photocatalytic activity, J. Alloys Compd. 746 (2018) 576–582.
[27] Z.Q. Li, Z. Li, Z. Shi, X.S. Fang, Facet-dependent, fast response, and broadband photodetector based on highly stable all-inorganic $CsCu_2I_3$ single crystal with 1D electronic structure, Adv. Funct. Mater. 30 (2020) 2002634.
[28] S. Li, Z. Ge, B. Zhang, Y. Yao, H. Wang, J. Yang, Y. Li, C. Gao, Y. Lin, Mechanochemically synthesized sub-5 nm sized CuS quantum dots with high visible-light-driven photocatalytic activity, Appl. Surf. Sci. 384 (2016) 272–278.
[29] W. Liang, M.-H. Whangbo, Conductivity anisotropy and structural phase transition in covellite CuS, Solid State Commun. 85 (5) (1993) 405–408.
[30] S.W. Goh, A.N. Buckley, R.N. Lamb, Copper(II) sulfide? Miner. Eng. 19 (2) (2006) 204–208.
[31] H. Zhang, H. He, X. Jiang, Z. Xia, W. Wei, Preparation and characterization of chiral transition-metal dichalcogenide quantum dots and their enantioselective catalysis, ACS Appl. Mater. Interfaces 10 (36) (2018) 30680–30688.
[32] V. Vinod Kumar, P.S. Hariharan, D. Eniyavan, N. Hari, S.P. Anthony, Alanine based coordinating ligand mediated hydrothermal synthesis of CuS nano/microstructures and morphology dependent photocatalysis, CrystEngComm 17 (18) (2015) 3452–3459.
[33] Y. Li, J. Cheng, J. Li, X.i. Zhu, T. He, R. Chen, Z. Tang, Tunable chiroptical properties from the plasmonic band to metal–ligand charge transfer band of cysteine-capped molybdenum oxide nanoparticles, Angew. Chem. Int. Ed. Engl. 130 (32) (2018) 10393–10397.
[34] M. Ahmed, M.S. Iqbal, Solid-state synthesis and characterization of copper–penicillamine complexes, Inorg. Nano-Met. Chem. 47 (6) (2017) 818–823.
[35] X. Qiu, J. Hao, J. Li, Z. Gong, S. Li, J. Cheng, X. Lin, T. He, Strong multiphoton absorption in chiral CdSe/CdS dot/rod nanocrystal-doped poly (vinyl alcohol) films, Opt. Lett. 44 (2019) 2256–2259.
[36] J. Cheng, J. Hao, H. Liu, J. Li, J. Li, X.i. Zhu, X. Lin, K. Wang, T. He, Optically active CdSe-dot/CdS-rod nanocrystals with induced chirality and circularly polarized luminescence, ACS Nano 12 (6) (2018) 5341–5350.
[37] J. Kuno, Y. Imamura, M. Katouda, M. Tashiro, T. Kawai, T. Nakashima, Inversion of optical activity in the synthesis of mercury sulfide nanoparticles: role of ligand coordination, Angew. Chem. Int. Ed. Engl. 57 (37) (2018) 12022–12026.
[38] W. Ma, J. Mao, C. Hao, L. Xu, C. Xu, H. Kuang, Chiral semiconductor nanorod heterostructures with high photocatalysis activity, Appl. Catal. B. 245 (2019) 691–697.
[39] A. Nain, S.-C. Wei, Y.-F. Lin, Y.-T. Tseng, R.P. Mandal, Y.-F. Huang, C.-C. Huang, F.-G. Tseng, H.-T. Chang, Copper sulfide nanoassemblies for catalytic and photoresponsive eradication of bacteria from infected wounds, ACS Appl. Mater. Interfaces 13 (7) (2021) 7865–7878.
[40] Y.a. Zhou, H. Sun, H. Xu, S. Matysiak, J. Ren, X. Qu, Mesoporous encapsulated chiral nanogold for use in enantioselective reactions, Angew. Chem. Int. Ed. Engl. 130 (51) (2018) 17033–17037.
[41] W. Yun, J. Park, D. Lim, C. Ahn, I. Sun, K. Kim, How did conventional nanoparticle-mediated photothermal therapy become "hot" in combination with cancer immunotherapy? Cancers 14 (2022) 2044.
[42] L. Wang, X. Ma, K. Cai, X. Li, Morphological effect of copper sulfide nanoparticles on their near infrared laser activated photothermal and photodynamic performance, Mater. Res. Express 6 (2019), 105406.
[43] W. Chen, Y.i. Xie, C. Hu, T. Zeng, H. Jiang, F. Qiao, J. Gu, X. Dong, X. Zhao, Room temperature synthesis of aqueous soluble covellite CuS nanocrystals with high photothermal conversion, CrystEngComm 20 (30) (2018) 4283–4290.

[44] G. Yang, M. Kazes, D. Oron, Chiral 2D colloidal semiconductor quantum wells, Adv. Funct. Mater. 28 (2018) 1802012.
[45] X. Shao, T. Zhang, B. Li, Y. Wu, S. Li, J. Wang, S. Jiang, Controllable chiral behavior of type-II core/shell quantum dots adjusted by shell thickness and coordinated ligands, Chirality 33 (4) (2021) 167–175.
[46] S. Xiao, J. Liang, J. Li, J. Cheng, X.i. Zhu, T. He, Tunable optical activities in chiral transition metal oxide nanoparticles, Nanoscale 14 (41) (2022) 15414–15421.
[47] J. Lin, R. Liu, X. Zhu, A. Wei, X. Xu, T. He, J. Cheng, Y. Li, Chiroptical transitions of enantiomeric ligand-activated nickel oxides, Small 18 (2022) 2107570.
[48] A. Ben Moshe, D. Szwarcman, G. Markovich, Size dependence of chiroptical activity in colloidal quantum dots, ACS Nano 5 (11) (2011) 9034–9043.
[49] U. Tohgha, K.K. Deol, A.G. Porter, S.G. Bartko, J.K. Choi, B.M. Leonard, K. Varga, J. Kubelka, G. Muller, M. Balaz, Ligand induced circular dichroism and circularly polarized luminescence in CdSe quantum dots, ACS Nano 7 (12) (2013) 11094–11102.
[50] A.O. Govorov, Z. Fan, P. Hernandez, J.M. Slocik, R.R. Naik, Theory of circular dichroism of nanomaterials comprising chiral molecules and nanocrystals: plasmon enhancement, dipole interactions, and dielectric effects, Nano Lett. 10 (2010) 1374–1382.
[51] N. Gharda, M. Galai, L. Saqalli, M. Ouakki, N. Habbadi, R. Ghailane, A. Souizi, M. E. Touhami, Y. Peres-lucchese, Synthesis, structural properties and complex corrosion inhibition Cu (II) with amino acid (DL-α-Alanine), Orient. J. Chem. 33 (2017) 1665–1676.
[52] Y.A. Joh, Y.H. Kwon, S. Tannir, B.M. Leonard, J. Kubelka, K. Varga, M. Balaz, The effect of molecular isomerism on the induced circular dichroism of cadmium sulfide quantum dots, J. Mater. Chem. C 9 (48) (2021) 17483–17495.
[53] S. Jiang, M. Chekini, Z. Qu, Y. Wang, A. Yeltik, Y. Liu, A. Kotlyar, T. Zhang, B. Li, H.V. Demir, N.A. Kotov, Chiral ceramic nanoparticles and peptide catalysis, J. Am. Chem. Soc. 139 (2017) 13701–13712.
[54] V.K. Valev, J.J. Baumberg, C. Sibilia, T. Verbiest, Chirality and chiroptical effects in plasmonic nanostructures: fundamentals, recent progress, and outlook, Adv. Mater. 25 (2013) 2517–2534.